Effect of Mn-doping on the growth mechanism and electromagnetic properties of chrysanthemum-like ZnO nanowire clusters*

Yan Jun-Feng(闫军锋)[a)b)], You Tian-Gui(游天桂)[a)], Zhang Zhi-Yong(张志勇)[a)b)†], Tian Jiang-Xiao(田江晓)[a)], Yun Jiang-Ni(员江妮)[a)b)], and Zhao Wu(赵 武)[a)b)]

[a)] *School of Information Science and Technology, Northwest University, Xi'an* 710069, *China*

[b)] *Key Laboratory of Optoelectronic Technology of Shaanxi Province, Northwest University, Xi'an* 710069, *China*

(Received 28 September 2010; revised manuscript received 7 December 2010)

Chrysanthemum-like ZnO nanowire clusters with different Mn-doping concentrations are prepared by a hydrothermal process. The microstructure, morphology and electromagnetic properties are characterized by x-ray diffractometer high-resolution transmission electron microscopy (HRTEM), a field emission environment scanning electron microscope (FEESEM) and a microwave vector network analyser respectively. The experimental results indicate that the as-prepared products are Mn-doped ZnO single crystalline with a hexagonal wurtzite structure, that the growth habit changes due to Mn-doping and that a good magnetic loss property is found in the Mn-doped ZnO products, and the average magnetic loss tangent $\tan\delta_{\rm m}$ is up to 0.170099 for 3% Mn-doping, while the dielectric loss tangent $\tan\delta_{\rm e}$ is weakened, owing to the fact that ions Mn^{2+} enter the crystal lattice of ZnO.

Keywords: chrysanthemum-like ZnO nanowire clusters, electromagnetic properties, hydrothermal method, Mn-doping

PACS: 81.10.Dn, 81.07.Gf, 81.16.Dn, 77.22.Gm **DOI:** 10.1088/1674-1056/20/4/048102

1. Introduction

With the increasing use of gigahertz electromagnetic waves in industrial, commercial and military fields, electromagnetic pollution has become a serious problem and a matter of crucial concern recently.[1] Thus electromagnetic wave absorption materials have attracted considerable attention.[2] However, conventional electromagnetic absorption materials, such as ferrite and conductive fibres, each have fairly high densities, which restricts their application in some specialized areas.[3,4] Extensive study has been carried out to develop new absorption materials with strong absorptions in a wide frequency range, low density and high resistivity.[5]

With a wide direct bandgap, strong excitonic binding energy and controllable morphology, nanostructured ZnO should be a good candidate for a new absorption material due to its light weight, high surface-to-volume ratio and superior semiconductor properties. The research teams of Zhou,[6] Cao,[7−11] Zhang,[12−14] Yan[1,15,16] and Cao[17] have all deeply investigated the electromagnetic wave absorption properties of nanostructured ZnO with specific morphologies such as tetraneedle-like ZnO whiskers, cage-like ZnO particles, ZnO nanowires, ZnO nanotrees, and so on. It is evident that almost all of this research was focused on pure ZnO with no magnetic loss, and that most of them involved preparation methods at high temperatures with a low number of finished products. In our previous work,[18,19] we fabricated chrysanthemum-like ZnO nanowire clusters with uniform morphology through a hydrothermal process at low temperature and investigated the nucleation mechanism and the effect of polyacrylamide on their morphology and electromagnetic properties.

In the present study, in order to improve the electromagnetic properties of chrysanthemum-like ZnO nanowire clusters, we design and prepare some chrysanthemum-like Mn-doped ZnO nanowire clusters and investigate their electromagnetic properties in detail. Importantly, a ZnO product with a good magnetic loss property was obtained.

*Project supported by the National Natural Science Foundation of China (Grant No. 60976069), the Natural Science Foundation of Shaanxi Province, China (Grant No. 2010JM6008), and the Xi'an Scientific and Technological Project, China (Grant No. CXY1008).

†Corresponding author. E-mail: Zhangzy@nwu.edu.cn

© 2011 Chinese Physical Society and IOP Publishing Ltd

2. Experiment

In the experiment, deionized water was used as the solvent and an appropriate sodium hydroxide (NaOH) solution was added to the mix liquid of zinc acetate dihydrate ($Zn(CH_3COO)_2{\cdot}2H_2O$) and manganese acetate tetrahydrate ($Mn(CH_3COO)_2{\cdot}4H_2O$), accompanied with a cold water bath and stirring, which formed a transparent and stable precursor. The final concentrations of the raw materials in the precursor are listed in Table 1. The precursor was then put into an autoclave with a Teflon lining, the compactedness of which was around 70%. After that, the autoclave was put into a bake oven and the temperature maintained at 200 °C for 12 h. Finally, the products were kept scoured and filtered until the PH value of the filtrate reached 7 and then dried at 60 °C in air for further characterization.

Table 1. Final concentrations of the raw materials in the precursor and the lattice constant of as-prepared products (1 Å = 0.1 nm).

sample	$[Zn^{2+}]$/(mol/L)	$[OH^-]$/(mol/L)	ratio of $[Mn^{2+}]$ to $[Zn^{2+}]$	a/Å	c/Å	c/a
1	0.1	1.4	0	3.2511	5.2191	1.6053
2	0.1	1.4	1%	3.2562	5.2195	1.6029
3	0.1	1.4	3%	3.2571	5.2181	1.6021
4	0.1	1.4	5%	3.2561	5.2138	1.6012

The microstructure and morphology of the ZnO products were examined using an x-ray diffraction meter (D/Max2550VB+/PC, Rigaku, Japan), an HRTEM (JEM-3010, JEOL, Japan) and an FEESEM (Quanta 400 FEG, FEI, Holand), respectively. The ZnO particles/paraffin composites were prepared by dispersing ZnO with a weight ratio of 20% into paraffin, which is transparent for microwave, and the electromagnetic parameters of the composites in the X band (8.2 GHz∼12.4 GHz) and the Ku band (12.4 GHz∼18 GHz) were measured by a microwave vector network analyser (Agilent technologies E8362B, Agilent, America).

3. Results and discussion

3.1. Energy dispersive spectroscopy (EDS) and x-ray diffraction (XRD) analysis

The EDS measurement was carried out at a number of locations throughout the deposits under the scanning electron microscope (SEM). Figures 1(a) and 1(b) show the representative EDS spectra of the undoped product and the Mn-doped product (sample 2). It is obvious that there is Zn and O in all of the samples, and only Mn could be detected in the Mn-doped products.

Figure 2 shows the XRD patterns of the as-prepared products with different Mn-doping concentrations. The major diffraction peaks can be indexed according to the hexagonal wurtzite structure of ZnO (space group $p6_3mc$(186); JCPDS card No. 36-1451). Except for the MnO_2 and the $Mn_9Na_4O_{18}$ in sample 4, there is no detectable secondary phase. The lattice constants (a, c) are calculated as shown in Table 1. The values of c/a decrease with the increase of Mn-doping concentration, which implies that the Mn ions replace the Zn ions in the ZnO lattice.

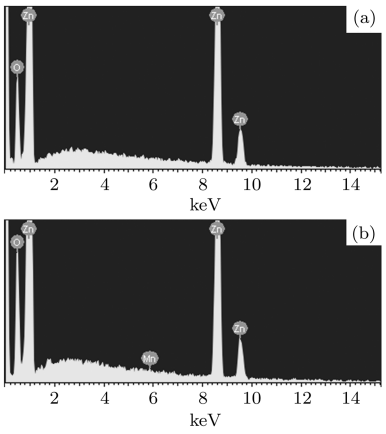


Fig. 1. EDS spectra of sample 1 (a) and sample 2 (b).

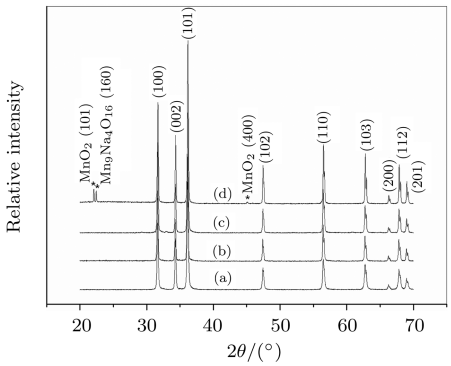


Fig. 2. The XRD patterns of as-prepared ZnO products: (a) sample 1, (b) sample 2, (c) sample 3, (d) sample 4.

3.2. HRTEM analysis of the as-prepared ZnO product

The HRTEM images of the nanowire taken from the as-prepared ZnO products are given in Fig. 3. Figure 3(a) shows a typical ZnO nanowire at 200 °C. The selected-area electron diffraction (SAED) pattern in Fig. 3(b) and the HRTEM image in Fig. 3(c) confirm that the ZnO nanowire is single crystalline with a hexagonal wurtzite structure and space group $p6_3mc$, and the growth direction is along [0001].

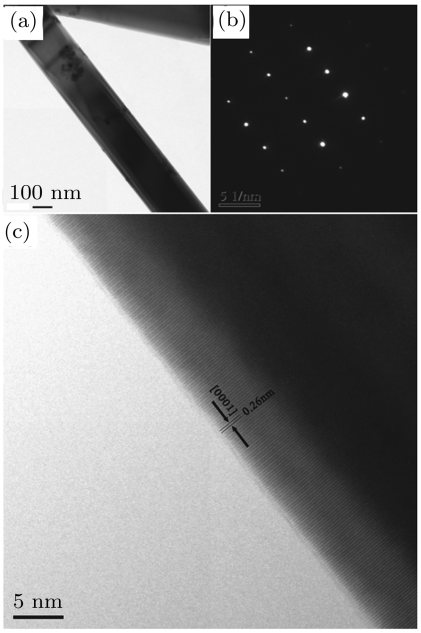


Fig. 3. (a) The HRTEM image of a nanowire taken from the as-prepared ZnO products, (b) the SAED image of the nanowire showing a [0001] growth direction, and (c) the HRTEM image taken from the lateral surface of the nanowire in (a).

3.3. Effect of Mn-doping on the growth mechanism of as-prepared ZnO products

A group of SEM images of the as-prepared ZnO products are shown in Figs. 4(a)–4(d), in which the inset indicates the corresponding higher magnification SEM image. By analysing Fig. 4, it is clear that all the as-prepared ZnO products with different Mn-doping concentrations have a three-dimensional chrysanthemum-like structure. However, the quantity of the petal-like nanowires in the Mn-doped chrysanthemum-like structure seems to be more than that in the undoped chrysanthemum-like structure. There are also some individual nanowires in the as-prepared Mn-doped products and this situation worsens, especially in sample 4, which implies that Mn-doping damages the chrysanthemum-like structure to a certain extent. The values of slenderness ratio $L_{\rm d}$[18,19] are 11.25, 9.50, 10.33 and 8.93 for samples 1, 2, 3 and 4, respectively. It is noticeable that Mn^{2+} has a great influence on the growth mechanism of chrysanthemum-like ZnO nanowire clusters.

The coupling interaction between Mn^{2+} ions with a spin magnetic moment and the basic crystalline growth cells $[Zn(OH)_4]^{2-}$ with an electric dipole moment effectively improves the $[Zn(OH)_4]^{2-}$ to fold together, thereby forming a ZnO crystal nucleus in the strong convection condition with a severe phase change process. Simultaneously, under the synergistic constraints of supersaturation, reacting temperature and systematical pressure, the nucleation density increases only within a certain limit. Therefore, the quantity of nuclei is slightly enhanced in the multi-twin central nucleus, which is a spherical aggregate with multiple nuclei that can adjust their state themselves under certain hydrothermal conditions. This results in an increase of petal-like nanowires in the Mn-doped chrysanthemum-like structure. As mentioned in Ref. [18], under an adequate environmental driving force, the c axis of an individual nucleus is uniformly arranged along the radial direction of the sphere in a multi-twin central nucleus. Thus, the multi-twin central nuclei with special internal structures form and further develop to form chrysanthemum-like ZnO nanowire clusters. When the concentration of Mn^{2+} is in a range from 1% to 3%, the quantity of petal-like nanowires in the chrysanthemum-like structure increases due to the fact that the above coupling interaction is enhanced, and owing to the presence of concentration gradient of Mn^{2+}, multi-twin central nuclei cannot form in areas of high Mn^{2+} concentration and the basic cells of crystalline growth $[Zn(OH)_2]^{2-}$ can fold together only on the individual nuclei, which results in individual nanowires being formed in Mn-doped samples. While the Mn^{2+} concentration increases to 5%, the excessive Mn^{2+} ions are restrained from the formation of the multi-twin central nucleus so as to form the coexistence phases of more individual nanowires and the chrysanthemum-like structure (see Fig. 4(d)).

The impurity of the Mn in the crystal lattice of ZnO impedes the (0001) preferential orientation of ZnO to some extent, so the values of $L_{\rm d}$ of Mn-doped ZnO are all smaller than those of the undoped products. While, with the increase of Mn-doping, more Mn^{2+} ions with a spin magnetic moment assemble around the non-polar surfaces of ZnO nanowires and restrict the growth of non-polar surfaces, so the rela-

tive growth rate between the positive polar axial surface and the non-polar lateral surface is increased in higher Mn-doping concentrations. Therefore, the L_d value of sample 3 is larger than that of sample 2. As to the smallest value of L_d in sample 4, that may result from the secondary phases of MnO_2 and $Mn_9Na_4O_{18}$.

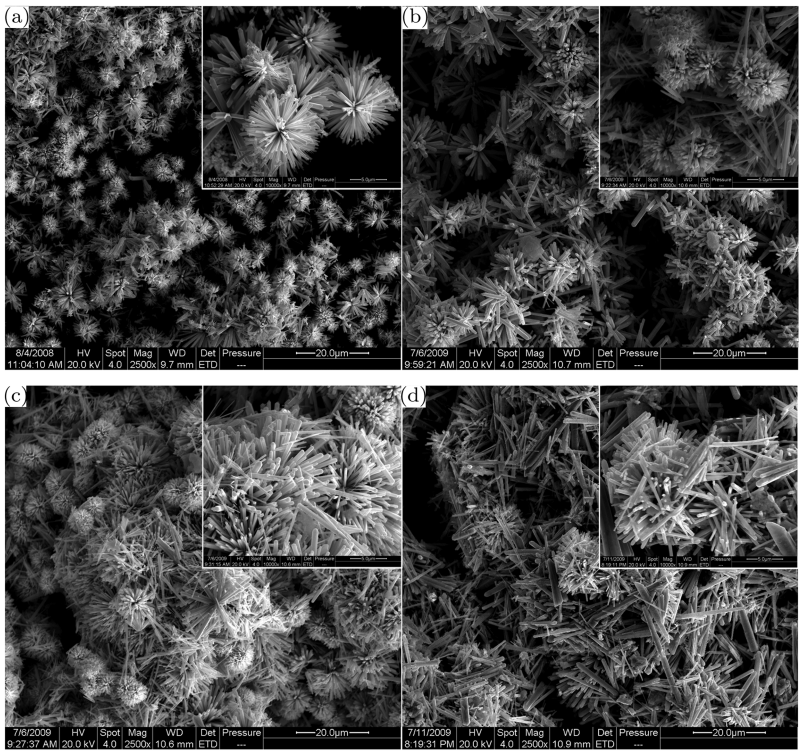


Fig. 4. FEESEM images of the as-prepared ZnO products: (a) sample 1, (b) sample 2, (c) sample 3 and (d) sample 4.

3.4. The effect of Mn-doping on the electromagnetic properties of chrysanthemum-like ZnO nanowire clusters

3.4.1. Dielectric properties

Figures 5(a)–5(c) show the real part of permittivity ε', the imaginary part of permittivity ε'' and the dielectric loss tangent $\tan\delta_e$ of samples 1, 2, 3 and 4 in X band and Ku band, respectively. Sample 4 has the smallest average value of ε' and there is no significant difference in the average value of ε' among samples 1, 2 and 3. The values of ε'' and $\tan\delta_e$ gradually increase with the increase of the L_d value discussed in Subsection 3.3, i.e., the larger the value of L_d, the better the dielectric properties will be. Obviously, all of the samples have better dielectric loss properties in the Ku band than in the X band.

The real part of permittivity ε', caused by displacement polarization, largely depends on the crystalline quality of the ZnO product. The 5% Mn-doping not only leads to the secondary phases of MnO_2 and $Mn_9Na_4O_{18}$ detected by XRD but also significantly damages the structural integrity of the ZnO crystalline, which hampers displacement polarization. So the value of ε' of sample 4 is the smallest. The dielectric loss tangent $\tan\delta_e$, defined as the ratio of ε'' to ε', represents the phase lag of the dipole oscillation with respect to the applied electric field and the contribution from the finite conductivity of the ZnO products. According to Refs. [18] and [19], it is clear that the dielectric loss mechanism of the ZnO products consists of the turning-direction polarization of the electric dipole, the associated relaxation phenomenon and the conducting network. The occupied Mn^{2+} cannot enhance the current carrier concentration in ZnO and they become scattering centres to current carriers instead. At the same time, as discussed in Subsection 3.3, Mn-doping destroys the chrysanthemum-like structure which easily forms a conducting network, so

as to decrease the conductivity of the dielectric and further reduce the dielectric loss tangent $\tan\delta_e$. In addition, the conclusion that the large value of L_d results in large dielectric loss tangent $\tan\delta_e$ has been confirmed in our previous work.[18,19] So the values of $\tan\delta_e$ are distinct from each other, as shown in Fig. 5(c). The turning-direction polarization and associated relaxation phenomenon of electric dipole will be more prominent at higher frequency. Therefore, the value of dielectric loss tangent $\tan\delta_e$ will be larger at higher frequencies.

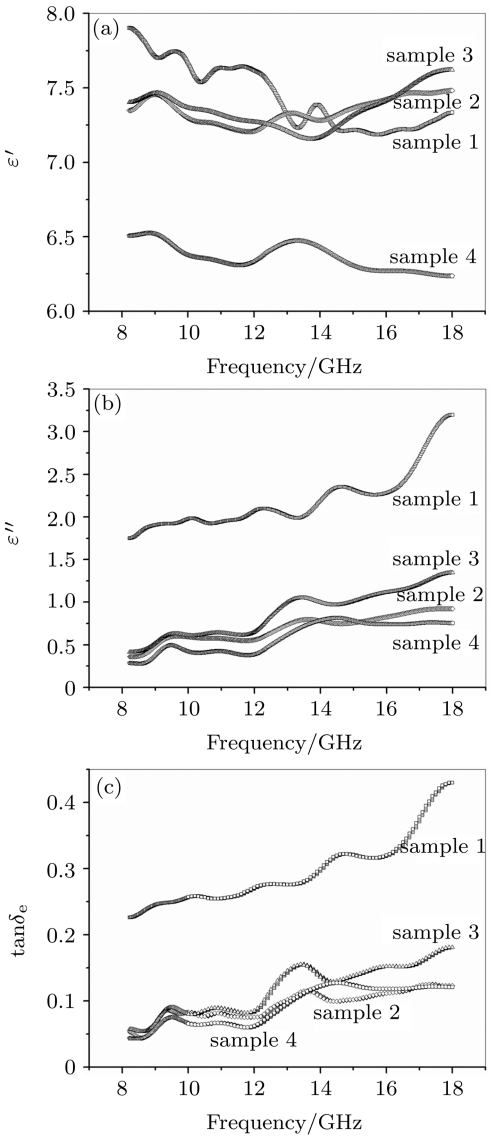


Fig. 5. (a) Real part of permittivity ε', (b) imaginary part of permittivity ε'', and (c) dielectric loss tangent $\tan\delta_e$.

3.4.2. Magnetic properties

Figures 6(a)–6(c) show the real and the imaginary parts of permeability (μ', μ'') and the values of the magnetic loss tangent $\tan\delta_m$ of samples 1, 2, 3 and 4 in the X band and the Ku band, respectively. The μ' values of all the samples seem to show a similar tendency and entwine each other, and the values of μ'' and $\tan\delta_m$ each show a decrease trend with increases of frequency, i.e., there is a better magnetic loss property in X band than in Ku band. The average values of μ'' and $\tan\delta_m$ increase in sequence of samples 1, 2, 4 and 3, and the average values of μ'' and $\tan\delta_m$ of sample 1 tend to be 0, that is to say, Mn-doping induces the magnetic loss property in ZnO.

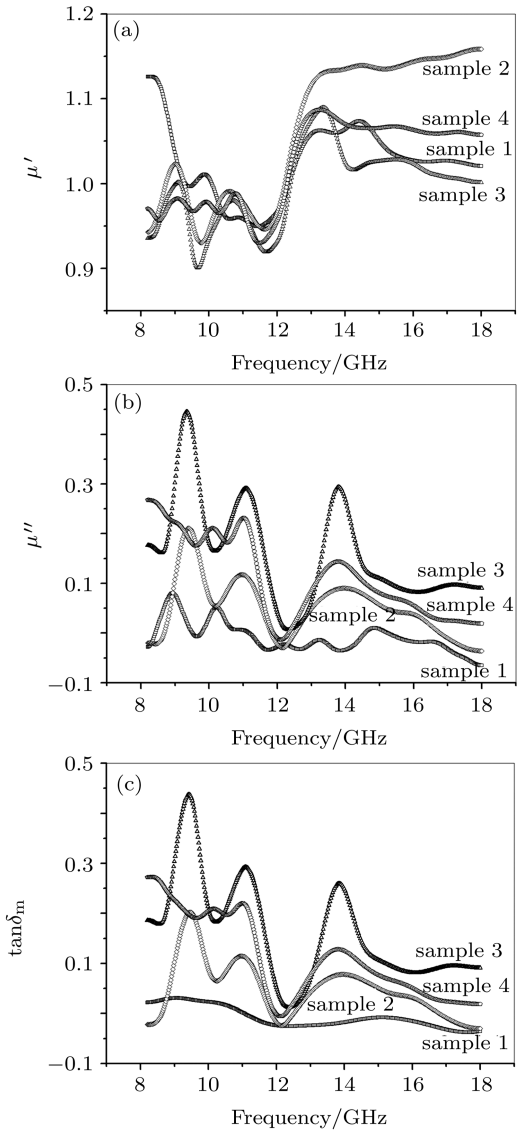


Fig. 6. (a) Real part of permeability μ', (b) imaginary of permeability μ'' and (c) magnetic loss tangent $\tan\delta_m$.

The magnetic loss tangent $\tan\delta_m$, defined as the ratio of μ'' to μ', represents the phase lag of the magnetic-dipole oscillation and the associated relaxation magnetization with respect to the applied magnetic field. According to Ref. [20], the occupied Mn^{2+} states in ZnO are fully polarized and the predicted

moment is 5 μ_B per Mn. The magnetic moments are ordered ferromagnetically and ferromagnetism will be suppressed when the Mn ions form high-concentration clusters. The magnetic property of the nano-structure will be enhanced, which will be reported in detail in a later work. There are more magnetic moments in the higher concentration of Mn-doped system, so the magnetic property will be stronger and the larger magnetic loss is natural. However, the magnetic property will be impeded when the Mn concentration is too high, i.e. 5%. Thus, it is found that sample 3 has the largest magnetic loss tangent $\tan\delta_m$. The frequency of magnetic-dipole oscillation is far lower than the frequency of the applied magnetic field in the X and Ku bands. The associated relaxation magnetization will be damped at high frequency. So the values of the magnetic loss tangent $\tan\delta_m$ show a decrease trend with frequency increasing.

4. Conclusion

Chrysanthemum-like ZnO nanowire clusters with different Mn-doping concentrations are prepared by a hydrothermal process. Their microstructures, morphologies and electromagnetic properties have been characterized. The Mn-doping changes the growth mechanism of the chrysanthemum-like ZnO nanowire clusters and weakens the dielectric loss property of ZnO, but induces good magnetic loss property, which tends to 0 in undoped ZnO. There is good dielectric loss at a high frequency (Ku band) and good magnetic loss at a low frequency (X band) when the Mn-doping concentration is 3%. This suggests that Mn-doping can broaden the absorber bandwidth and improve the electromagnetic wave absorption property of chrysanthemum-like ZnO nanowire clusters, which may be important in the design of high-performance microwave absorption materials.

References

[1] Zhou R F, Qiao L, Feng H T, Chen J T, Yan D, Wu Z G and Yan P X 2008 *J. Appl. Phys.* **104** 094101

[2] Li G, Hu G, Zhou H, Fan X and Li X 2002 *Mater. Chem. Phys.* **75** 101

[3] Hatakeyama K and Inui T 1984 *IEEE Trans. Magn.* **20** 1261

[4] Matsumoto M and Miyata Y 1997 *IEEE Trans. Magn.* **33** 4459

[5] Liu X G, Geng D Y, Meng H, Shang P J and Zhang Z D 2008 *Appl. Phys. Lett.* **92** 173117

[6] Zhou Z W, Chu L S and Hu S C 2006 *Mater. Sci. Eng.* B **126** 93

[7] Chen Y J, Cao M S, Wang T H and Wan Q 2004 *Appl. Phys. Lett.* **84** 3367

[8] Cao M S, Shi X L, Fang X Y, Jin H B, Hou Z L, Zhou W and Chen Y J 2007 *Appl. Phys. Lett.* **91** 203110

[9] Shi X L, Yuan J, Zhou W, Rong J L and Cao M S 2007 *Chin. Phys. Lett.* **24** 2994

[10] Zhou Y, Shi X L, Yuan J, Fang X Y and Cao M S 2007 *Chin. Phys. Lett.* **24** 3264

[11] Huang Y Q, Yuan J, Song W L, Wen B, Fang X Y and Cao M S 2010 *Chin. Phys. Lett.* **27** 027702

[12] Cao J W, Huang Y H, Zhang Y, Liao Q L and Deng Z Q 2008 *Acta Phys. Sin.* **57** 3641 (in Chinese)

[13] Li H F, Huang Y H, Sun G B, Yan X Q, Yang Y, Wang J and Zhang Y 2010 *J. Phys. Chem.* C **114** 10088

[14] Wang J, Li H F, Huang Y H, Yu H B and Zhang Y 2010 *Acta Phys. Sin.* **59** 1946 (in Chinese)

[15] Zhou R F, Feng H T, Chen J T, Yan D, Feng J J, Li H J, Geng B S, Cheng S, Xu X Y and Yan P X 2008 *J. Phys. Chem.* C **112** 11767

[16] Zhou R F, Feng H T, Liang Q, Liu J Z, Chen J T, Yan D, Feng J J, Li H J, Cheng S, Geng B S, Xu X Y, Wang J, Wu Z G, Yan P X and Yue G H 2008 *J. Phys.* D: *Appl. Phys.* **41** 185405

[17] Huang Y X, Cao Q X, Li Z M, Jinag H Q, Wang Y P and Li G F 2009 *J. Am. Ceram. Soc.* **92** 2129

[18] Yan J F, Zhang Z Y, You T G, Zhao W and Yun J N 2009 *Chin. Phys.* B **18** 4019

[19] Yan J F, Zhang Z Y, You T G, Zhao W, Yun J N and Zhang F C 2009 *Chin. Phys.* B **18** 4552

[20] Sharma P, Gupta A, Rao K V, Owens F J, Sharma R, Ahuja R, Guillen J M O, Johansson B and Gehring G A 2003 *Nature Mater.* **2** 673